Disorder Trapping During the Solidification of βNi_3Ge from its Deeply Undercooled Melt

R. Ahmad [1], *R.F. Cochrane & A.M. Mullis* [2]

Institute for Materials Research, University of Leeds, Leeds LS2-9JT, UK.

Abstract

A melt encasement (fluxing) technique has been used to solidify the congruently melting intermetallic βNi_3Ge from its deeply undercooled parent melt. High speed photography and a photo-diode technique have been used to measure the resulting growth velocity. The maximum undercooling achieved was 362 K, wherein a growth velocity of 3.55 m s^{-1} was recorded. At an undercooling of 168 K an abrupt increase in the gradient of the velocity-undercooling curve is observed and this is attributed to a transition from growth of the ordered $L1_2$ compound at low undercooling, to growth of the fully disordered compound at high undercooling. A change in the microstructure, from a distribution of very coarse (700 μm), randomly oriented grains to a fine grained structure (15-20 μm) with a large number of low angle grain boundaries is observed coincident with this transition in the velocity-undercooling curve, a grain refinement pattern that is different to that observed either in deeply undercooled solid solutions or other intermetallics. This transition is ascribed to a recovery and recrystallisation process in the disordered phase due to the low post-recalescence cooling rate.

Keywords: intermetallics, rapid solidification, disordered systems, microstructure.

[1] Permanent address: Mechanical Engineering Department, Faculty of Engineering, University Malaya, 50603 Kuala Lumpur, Malaysia.

[2] Corresponding author: Tel: +44 113 343 2568, Fax: +44 113 343 2384.

1. Introduction

Practical interest in intermetallics centres on their potential utilisation as high temperature structural materials due to their high hardness and good chemical stability at elevated temperature. However, a major drawback is their lack of room temperature ductility, which inhibits formability. One potential route to mitigate against this limitation is non-equilibrium processing of the intermetallic [1], such as by rapid solidification. Increased chemical disorder or a fine pattern of antiphase domains (APD's) increases ductility, making it less difficult to machine or forge to near net shape at room temperature. Upon subsequent annealing the chemical ordering and hence the high temperature properties of the material may be restored.

In the case of a conventional, disordered, solid solution the loss of local interface equilibrium during rapid growth leads to solute trapping, with the composition of the solid at the interface approaching that of the liquid. In the case of compositional variations, this deviation from thermodynamic equilibrium is measured by the partition coefficient [2]. Analogously, Boettinger and Aziz [3] have developed a model to describe disorder trapping during rapid solidification of intermetallic compounds. The formation of an ordered superlattice in the intermetallic compound requires short-range diffusion of atoms. If the growth velocity approaches the speed of atomic diffusion, disorder becomes progressively entrapped leading to the formation of a disordered compound. Just as we may use the variation of the partition coefficient to quantify departure from equilibrium by solute trapping, the long-range order parameter may be used to quantify the departure from equilibrium by disorder trapping [4]. For a binary compound, the long-range order parameter, η, may be defined as

$$\eta = \frac{r_A - X_A}{1 - X_A}$$

where X_A is the mole fraction of atoms of species A in the alloy and r_A is the probability that the A sublattice site is occupied by the correct atom type. η varies from 0 (complete random distribution) to 1 (fully ordered) [5].

In studying the effect of disorder trapping within intermetallics, congruently melting compounds are particularly attractive as, even during equilibrium solidification, a melt at the correct stoichiometry for the compound will solidify without partitioning. Disorder trapping may therefore be studied without the complication of considering simultaneous solute trapping. The main prediction of the Boettinger and Aziz [3] model for such a congruently melting compound is that η will decrease with increasing solidification velocity as progressively higher levels of chemical disorder are trapped in the structure. Such transitions may be thermodynamically either first or second-order. For thermodynamically first-order transitions, in which the ordered and disordered phases can co-exist in equilibrium, η will decrease continuously with increasing growth velocity v, up to some critical velocity v_T, wherein η will drop discontinuously to zero for velocities in excess of v_T [6]. Conversely, for thermodynamically second-order transitions, in which co-existence of the ordered and disordered phases is not permitted, it is expected that η will decrease continuously with increasing growth velocity until a completely disordered solution is obtained ($\eta = 0$).

In the case of second-order transitions this critical velocity, v_T, is related to the diffusive velocity, v_D, via the relationship

$$v_T = v_D\left[\left(T_C / T_M\right) - 1\right]$$

where T_M is the melting temperature and T_C is the critical temperature at which the free energies of the ordered and disordered solid phases are equal. Here, as indicated by the phase diagram, we take $T_C > T_M$, so that during equilibrium solidification the solid will grow in the ordered state directly from the liquid.

A model for the dendritic growth of intermetallic compounds by Assadi & Greer [7], taking into account both disorder trapping and complex partitioning behaviour, suggests that the growth velocity, v, will rise sharply at the point where the growing solid becomes completely disordered. The model appears to be borne out by the observations of Herlach [8] for the intermetallic CoSi, in which the growth velocity displayed a very abrupt increase in gradient with undercooling at a critical undercooling around 310 K, corresponding to a critical growth velocity of $\approx$3.8 m s^{-1}. This abrupt increase in growth velocity is modelled well by assuming a transition from diffusion limited growth of the ordered compound below v_T to collision limited growth of the disordered compound above v_T.

Following formation of a disordered solid due to growth at high velocity, some degree of reordering may take place during the period the material is at elevated temperature immediately following recalescence. The extent of the reordering depends critically upon the post-recalescence cooling rate and may give rise to the formation of anti-phase domains. Such domains arise from the fact that the transformation from a disordered structure to an ordered one proceeds via the formation of small ordered domains. A particular chemical species within a given domain will choose a sublattice that is different from that chosen by the same species in a neighbouring domain. As the domains increase in size and subsequently impinge, the interface between two domains of different ordering will constitute an anti-phase boundary (APB). In first-order transitions this requires a nucleation event to initiate growth of the ordered domain although in second-order transitions such ordering can occur spontaneously. APD's are normally much finer in scale than the grain structure of the material. A reduced degree of order and a fine distribution of anti-phase domains will increase the ductility of intermetallic compounds [1, 9].

The general effect of post recalescence cooling rate on the final structure of the as-solidified material has been described by Greer & Assadi [10]. Above a critical cooling rate, $\dot{T}_a$, a fully disordered solid is initially formed from the melt but can order to give anti-phase domains, which will generally be columnar in nature. Above a higher critical cooling rate, $\dot{T}_b$, the ordered domains will generally become equiaxed, rather than columnar, while for ultra-rapid cooling [11] there exists a critical cooling rate, $\dot{T}_c$, above which all re-ordering in the solid is suppressed. However, [10] caution that not all materials may display all stages in this sequence, or that some may undergo a transition to a glassy solid before complete disorder trapping can occur [12].

Based on the equilibrium phase diagram for this system [13], the Ni-rich portion of which is reproduced as Figure 1, βNi_3Ge is a congruently melting compound with a melting point of 1405 K. The homogeneity range is 22.5-25.0 at% Ge. In this paper we report upon rapid solidification experiments conducted on a Ni-24 at% Ge alloy performed using a melt encasement (fluxing) technique. This composition is (slightly) Ge-rich relative to the centre of the homogeneity range (23.75 at% Ge), thus providing a good compromise between ensuring that the composition falls within the single-phase stability field and providing a congruently melting compound (note from the phase diagram that the most Ge-lean compositions are not fully congruent). However, for this composition we would expect single-phase βNi_3Ge to be formed, irrespective of melt undercooling. As such this system offers a potentially attractive means of studying order-disorder transformations in intermetallic compounds without the complicating issues of competing metastable phase formation. The βNi_3Ge compound has an ordered fcc $L1_2$ (Cu_3Au) crystal structure, belonging to the $Pm\bar{3}m$ space group.

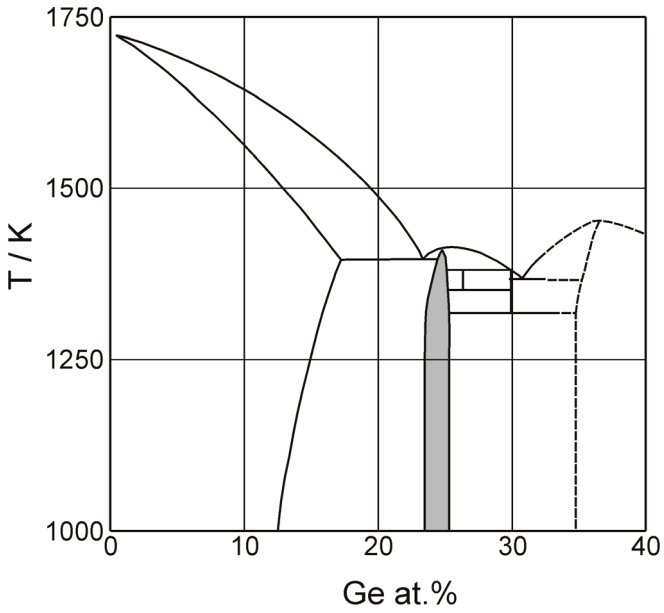

Figure 1 Ni-rich portion of the Ni-Ge phase diagram, showing (shaded) the congruently melting intermetallic βNi_3Ge

This structure is common to a number of intermetallics with composition X_3Y, as the fcc unit cell naturally accommodates 1 atom per cell at the cell corners and 3 atoms per cell on the cell faces. A number of important intermetallics with potential high temperature structural applications share the same $L1_2$ crystal structure. These include γ' Ni_3Al [14], Al_3Ti [15], in which the normal $D0_{22}$ structure can be modified to $L1_2$ by the addition of a number of dopants, including Cr, Mn, Fe and Co, Al_3Sc [16] and Pt_3Al [17]. Understanding the kinetics of the order-disorder transformation in this relatively simple model system may therefore provide useful insights into the behaviour of these more complex compounds.

Very little work exists on the solidification of the Ni-Ge system. Fang & Schulson [18] studied the gas atomisation and subsequent extrusion into bars of Ni_3Ge, although their alloy was doped with 0.06 at% of boron and most of their metallographic

analysis was concerned with the segregation of this boron and the subsequent formation of nickel boride precipitates. Such boron additions are generally made to increase ductility, and while this has been shown to be the case for Ni_3Si, Ni_3Ge generally remains brittle with such additions [19].

Detailed undercooling studies have been made on the closely related Fe-Ge system, at compositions of Fe-25 at% Ge [20] and Fe-18 at% Ge [21], the former of which is stoichiometric with the Fe_3Ge compound, while the latter solidifies to the ordered α-phase. At low undercooling both compositions appear to grow as an ordered compound and Fe-18 at% Ge, like CoSi, displays an abrupt increase in growth velocity above a critical undercooling that would be consistent with a transition from diffusion to collision-limited growth. This transition has not been observed in the Fe_3Ge compound, but this may be because the maximum undercooling achieved in this system ($\Delta T = 190$ K) was insufficient to mediate the transition. However, the Fe_3Ge system is much more complex than Ni_3Ge and so cannot be considered a direct analogue for βNi_3Ge. εFe_3Ge, which has an ordered hexagonal $D0_{19}$ structure, forms via the peritectic reaction $L + \alpha_2 \rightarrow \varepsilon$, where α_2 is an ordered B2 phase. Moreover, ε is dimorphic undergoing a transition to ε' which, like βNi_3Ge, has an ordered $L1_2$ structure.

Pure Ge also undergoes an abrupt rise in growth velocity above $\Delta T = 170$ K, corresponding to a growth velocity of 0.3 m s^{-1}, although in this case it is thought the jump is due to a transition from faceted to continuous growth brought about by kinetic roughening at elevated growth velocity [22, 23]. This process appears to be aided by the addition of small quantities of Fe [22].

2. Experimental Method

The Ni- 24 at% Ge alloy for the undercooling experiments was produced by weighing and mixing elemental Ni and Ge of 99.999% purity (metals basis). The mixture was then formed into 10 mm pellets which were arc melted under an argon atmosphere. Arc melting of the pellets was repeated at least 10 times in order to ensure the homogeneity of the final product. The pellets were weighed subsequent to arc melting to ensure no loss of material.

Undercooling experiments were performed within a stainless steel vacuum chamber evacuated to a pressure of 5×10^{-4} Pa using a turbo-molecular pump backed by a two stage, oil sealed, rotary vane pump. After being evacuated at this pressure for two hours the vacuum chamber was isolated from the pumping system by means of a gate valve and backfilled to 5×10^4 Pa with N_2 gas. Samples, of mass ~ 1.5g, were heated in fused quartz crucibles, by induction heating of a graphite susceptor contained within an alumina shell. Viewing slots were cut in the susceptor and alumina to allow the sample to be viewed through a window in the chamber. Melt encasement, within a high purity B_2O_3 flux, was employed to reduce the number of potential heterogeneous nucleation sites allowing the attainment of high undercoolings. Prior to performing the undercooling experiments the B_2O_3 flux was dehydrated for one hour by heating to just below its melting point under high vacuum.

Temperature determination was by means of an R-type thermocouple positioned beneath the crucible, which had been thinned at the base so reducing the thermal lag

between the sample and thermocouple. Cooling curves were obtained with the aid of a chart recorder. A schematic diagram of the experimental apparatus is shown in Figure 2. By heating the sample to its melting temperature, cooling and repeating this procedure, it was found that melting temperatures were reproducible to within $\pm$ 5 K. During a typical undercooling experiment the alloy would be superheated to 200 K above its melting point and, in order to achieve the highest undercoolings reported here, several heating-cooling cycles would be performed. Once the desired undercooling was obtained solidification was nucleated by touching the sample surface with a thin alumina trigger needle that was pushed through the flux. The experimental method is described in more detail in [24, 25].

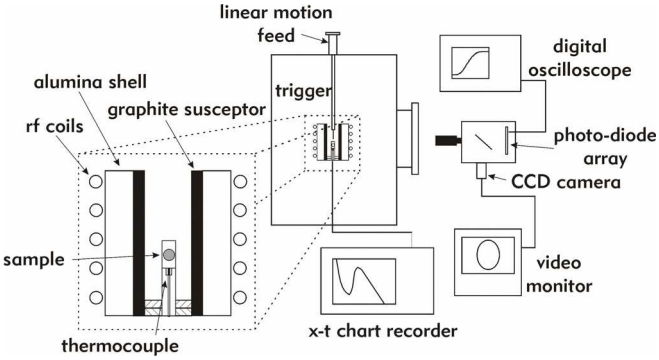

Figure 2 Schematic diagram of the melt fluxing apparatus used to undercool Ni-Ge (shown with apparatus for velocity measurement by photo-diode technique)

The measurement of growth velocities was performed using two independent methodologies. In the first, a 16 element linear photo-diode array was used, allowing the time taken for the bright recalescence front to move across the relatively dark sample to be measured. Light from the sample was passed through a beam splitter which distributed the light between a CCD camera and the photo-diode array. The CCD camera allows accurate sample positioning and focusing. It was also possible via this arrangement to measure directly the dimension of the sample along the photo-diode axis. A current proportional to the light intensity falling on each photo-diode is produced which was then amplified and recorded. Each of the 16 photo-diodes has an independent fast settling, low noise, DIFET amplifier with a current to voltage gain of 10^6 V A^{-1}. The signals are then passed, via switching circuitry, to a pair of voltage adders for output. The output signal is displayed as a light intensity vs time trace on a digital storage oscilloscope from which the time taken for the solidification front to move through the sample could be measured.

The second method for determining the growth velocity involved filming the progress of the recalescence front across the droplet at high (4500 fps) frame rate using a Kodak Ektapro 4050mx high speed motion analyser. As above, this allows the time taken for the solidification front to move across the sample to be measured. As with the photo-diode array, solidification of the sample was generally triggered by touching the sample with a fine alumina trigger needle pushed through the flux. However, at the highest undercoolings reported, unpredictable spontaneous nucleation of the sample became a problem. In these cases, and only when using the high speed motion analyser to obtain full frame images of the entire droplet, growth velocities

have been estimated from spontaneously nucleated samples provided the nucleation point could be unambiguously identified from the progress of the recalescence front.

Subsequent to the undercooling experiments microstructural characterisation of the samples has been conducted. Upon removal from the crucible the samples are in the form of slightly oblate spheroids, ~ 8 mm in diameter. XRD analysis using a PANalytical X'pert Pro HR-XRD facility has been used to confirm that the samples are single-phase, as expected from the phase diagram. Microstructural analysis was conducted using a Nikon Optishop optical microscope fitted with a Zeiss MRC5 Axiocam digital camera and a LEO 1530 Gemini FEGSEM (fitted with Oxford Instruments INCA EBSD software). Samples were sectioned through the trigger point (section plane parallel to the growth direction), mounted and polished flat for EBSD and XRD analysis, and were etched in a mixture of equal parts of hydrochloric, nitric and hydrofluoric acids to produce surface topography that could be imaged with the optical and scanning electron microscopes (secondary electron detection). TEM analysis has been conducted in order to determine whether anti-phase domain boundaries are present in the as-solidified samples, using a using a Philips CM20 transmission electron microscope operating at 200 kV. Due to the extreme brittleness of the samples, a Focused Ion Beam (FIB) linked to an FEI Nova 200 NanoLab FEGSEM was used to prepare the thin lamella samples with dimension 20 μm x 5 μm x 120 nm for TEM analysis.

3. Results

According to the equilibrium phase diagram for the Ni-Ge system (Fig. 1), solidification of the Ni- 24 at% Ge melt should result in the growth of single phase βNi_3Ge. To confirm this three samples have been subject to XRD analysis; an arc melted pellet and two samples undercooled by $\Delta T = 140$ K and 192 K (see Fig. 3). This XRD analysis confirms that both prior to, and following, undercooling experiments the material is indeed single phase βNi_3Ge. Differences in the relative peak intensities between the samples are apparent, however, we would caution that quantitative interpretation of the peak data is likely to be highly unreliable. Quantitative analysis requires a specimen that presents a very large number of randomly oriented grains to the X-ray beam, a condition that is not satisfied by the polished sections used here. The XRD analysis was undertaken to confirm that the material was single phase, and the technique employed is appropriate for this, but not for more detailed quantitative analysis. Specific differences between the XRD patterns for individual samples are likely to reflect differences between the methodologies used to obtain the samples. In particular, the arc melted sample does not display a (110) fundamental peak whereas the two undercooled samples do. However, in both undercooled samples the section is oriented relative to a well defined growth direction, whereas in the arc melted sample the growth direction is poorly defined as the sample was melted in a water-cooled copper hearth, which will have resulted in multiple heterogeneous nucleation across the entire lower surface of the sample. Similarly, between the samples undercooled by 140 and 192 K there are significant differences in the (220)/(110) and (222)/(111) peak ratios, but also very significant differences in the grain size which may make these ratios an unreliable guide to any texture within the sample. In particular, the grain size at lower undercooling (see below) is such that only a few grains may be exposed to the X-ray beam.

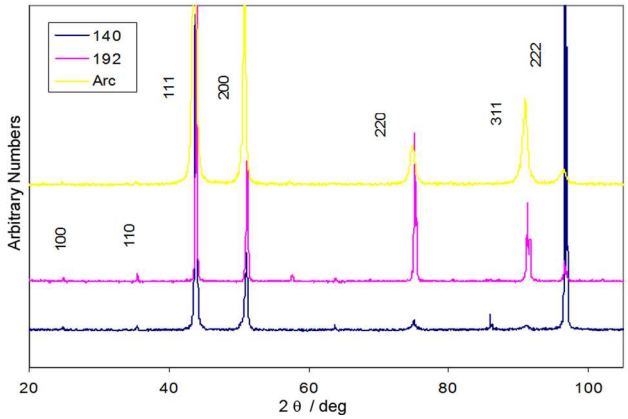

Figure 3 XRD analysis of an arc melted sample prior to undercooling (yellow) and samples undercooled by 140 K and 192 K (blue and purple) respectively

Figure 4a shows the measured velocity-undercooling curve for the Ni- 24 at% Ge alloy, with a magnified view of the low velocity portion of the curve being shown in Fig. 4b. It is clear from the curves that there is a high level of consistency between the three velocity determination methods used; triggered samples with the photo-diode detector, triggered samples with high speed photography and spontaneously nucleated samples with high speed photography. The highest undercooling achieved in this material was 362 K, wherein a growth velocity of 3.55 m s^{-1} was recorded. In common with other intermetallic compounds reported in the literature, there is an abrupt transition from the relatively slow, diffusion limited, growth of the ordered, or partially ordered, compound to the much faster, collision limited, growth of the fully disordered compound above a critical undercooling. In the case of βNi_3Ge this occurs at an undercooling of $\approx$ 168 K. At $\approx$ 0.22 m s^{-1}, the critical growth velocity, V_c, displayed by the ordered compound prior the transition to fully disordered growth is low, even when compared with measurements for other ordered intermetallic compounds such as CoSi (V_c = 3.8 m s^{-1}) [8] and Fe- 18 at% Ge (V_c = 0.75 m s^{-1}) [21]. For Fe_3Ge, the most closely analogous material to βNi_3Ge, the transition to collision limited growth was not observed even at the highest undercooling obtained (ΔT = 190 K) [20], with the maximum observed growth velocity being 1.3 m s^{-1}.

However, the critical velocity observed here is consistent with the growth velocity of *fully ordered* superlattice structures, maximum values for which are given in [26] as being in the range from 0.2 to 0.5 m s^{-1}. In contrast, the critical velocities observed in the systems CoSi and Fe_3Ge discussed above are significantly in excess of these values, particularly in the case of CoSi, which is also a congruently melting compound. The high critical velocity observed in CoSi may indicate that appreciable levels of disorder trapping are occurring prior to full disordering of the compound. Conversely, the relatively low critical velocity observed here for βNi_3Ge may indicate that little disorder trapping occurs prior to the transition to the fully disordered state. Unfortunately, there is insufficient thermodynamic data available for the Ni-Ge system to determine quantitatively whether the order-disorder transformation in this system will be first- or second-order, although the behaviour observed here may be more consistent with a first-order transition.

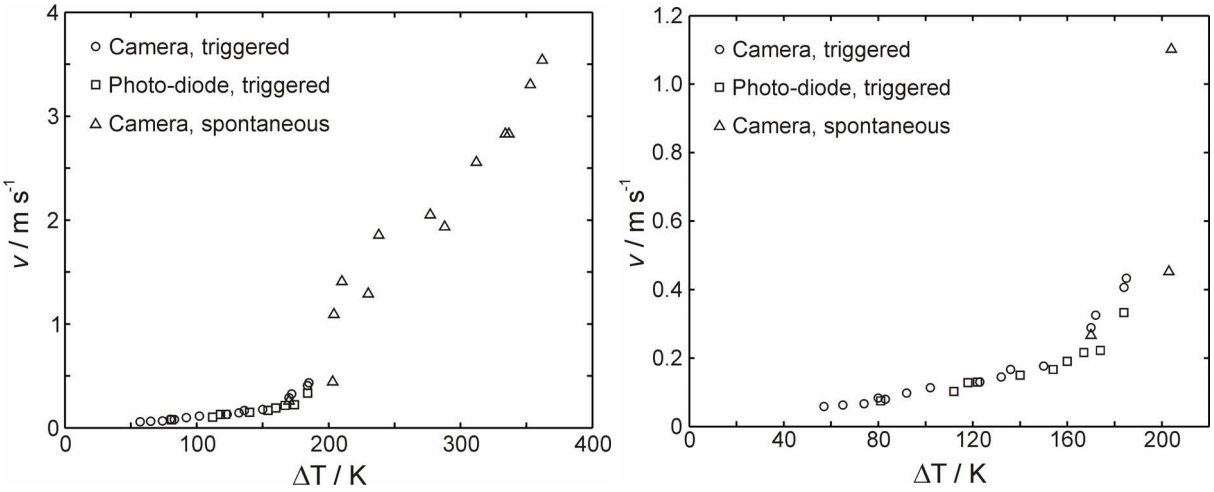

Figure 4 (a) Velocity-undercooling curve for the growth of βNi_3Ge and (b) detail from the low velocity, low undercooling region appropriate to the ordered $L1_2$ compound

From the velocity-undercooling curve we may identify two undercooling ranges for detailed microstructural characterisation; namely growth of the ordered compound for $57\ K \leq \Delta T \leq 168\ K$ and growth of the disordered compound for $168\ K \leq \Delta T \leq 362\ K$. Figure 5a shows a scanning electron micrograph of the ordered compound obtained using secondary electron detection to give topographic contrast. The sample undercooling prior to nucleation was, in this case, 74 K. The micrograph displays very coarse structures, typically 500-700 μm in diameter, which generally contain some degree of internal structure. In some, but not all, cases these comprises fine equiaxed components in the centre which then radiate outward, becoming coarser as they do so. Very similar structures are observed over the whole sample, with the microstructure shown being representative of the structure throughout the sample.

In order to examine whether there is any preferred crystallographic texture between neighbouring features in Fig. 5a EBSD mapping has been undertaken. Fig. 5b shows the EBSD texture map for the region indicated in Fig. 5a. In presenting this data we would point out that the two images were not obtained contemporaneously. The SEM image was obtained first, with the sample having been polished and etched. The sample was subsequently removed from the microscope and repolished in order to produce the flat surface required for EBSD mapping. The EBSD map shows a structure composed predominantly of equiaxed grains, with little evidence of the radial structures observed in the secondary electron image. Indeed, in many respects there appears to be little correspondence between the secondary electron image and the EBSD map. Moreover, careful analysis of the secondary electron image reveals areas of different grey level contrast, which we believe may correspond to different grains which have etched at slightly different rates. In some cases these appear to be cut by the boundaries of these radial features (see in particular the region to the left and below scale bar in Fig. 5a).

We therefore (perhaps tentatively) suggest that the sample solidified with an equiaxed grain structure as evident in the EBSD map, and that the structure observed in Fig. 5a is the result of extensive cracking during post-solidification shrinkage of the brittle intermetallic. In some regions of the sample, for instance on the right-hand margin of

Fig. 5a, the cracking appears to be predominantly intergranualer, which would be consistent with the 'pull-out' which is evident. However, elsewhere in the sample, as pointed out above, there may also be intragranular cracking. The radial features observed in Fig. 5a may therefore be radial crack patterns, where the radial cracking has been initiated by some impurity or structural defect acting as a stress concentrator. Figure 6 shows an optical micrograph, taken using differential interference contrast (DIC), which appears to show just such a radial crack pattern.

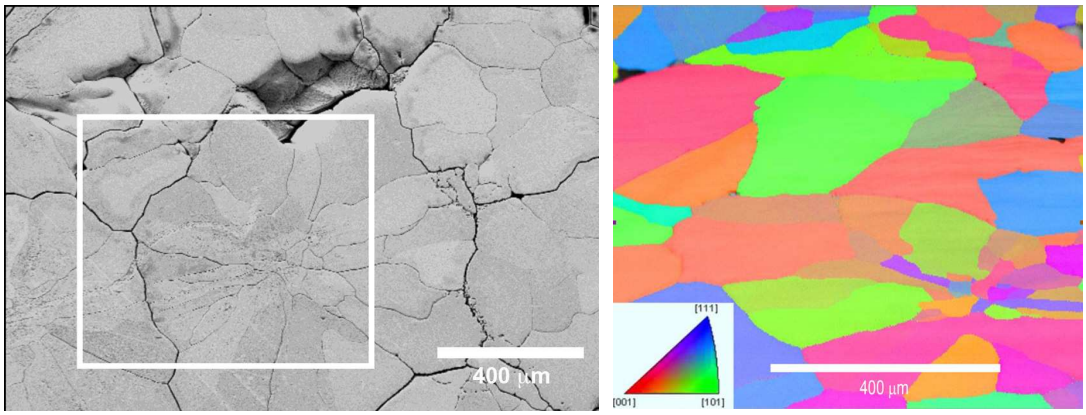

Figure 5 (a) SEM micrograph of a sample undercooled by 74 K prior to nucleation of solidification. The topographic image displays a coarse structure which appears to radiate from a number of point sources. (b) EBSD texture map of the region highlighted in (a). The radial structures evident topographically are not observed in EBSD map

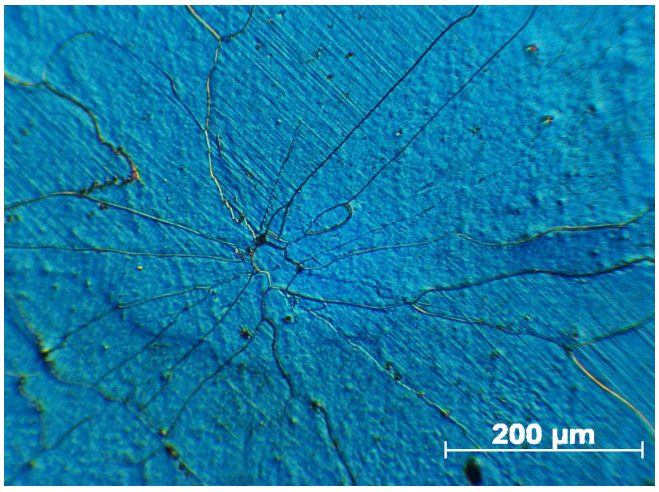

Figure 6 Optical micrograph of a sample undercooled by 74 K prior to nucleation of solidification displaying what appears to be a radial cracking pattern

The structures observed at low undercooling may be contrasted with those from the higher undercooling regime, as exemplified by Fig. 7, which was obtained from a sample undercooled by 170 K. The grain size is much finer (typically 15-20 µm) comprising exclusively equiaxed grains. A similar grain size distribution may be observed by viewing the unetched surface morphology (Fig. 8, sample undercooled by 194 K), although now it is evident that the majority of these grains also display a

straight line step morphology. These faceted features can be seen in more detail in Fig. 9, which was obtained by imaging through an open surface pore in a sample undercooled by 234 K. These features are not observed on the surface of samples undercooled by less than 168 K, nor on the surface of pellets obtained from arc melting. Interestingly, similar features have been observed [27] on droplets of pure Cu if the surface is clean enough. In this case the occurrence of such features has been attributed to the presence of residual compressive stress within the droplet arising from solidification shrinkage. A similar mechanism may give rise to the features observed here, with their occurrence being limited to the high undercooling regime, in which disordered growth occurs, by virtue of the ordered compound being too brittle to deform in this way. This morphology would therefore occur instead of the extensive cracking observed in the ordered compound at low undercooling and would comprise an alternative mechanism for accommodating the post-solidification shrinkage of the sample.

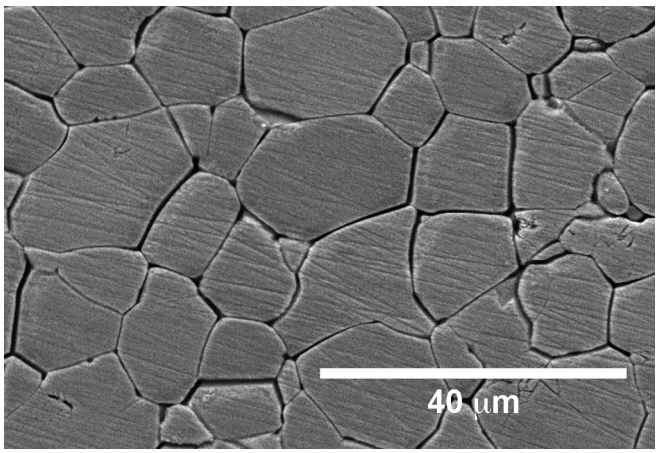

Figure 7 SEM micrograph of a sample undercooled by 170 K prior to nucleation of solidification, displaying highly refined microstructure

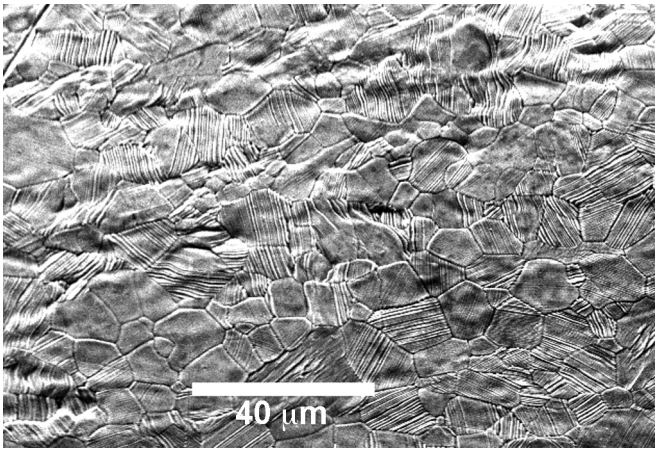

Figure 8 SEM micrograph of the surface morphology of a sample undercooled by 194 K prior to nucleation of solidification, displaying linear step like ledges on most grains

An EBSD map from a sample in the high undercooling regime (ΔT = 192 K) is shown in Fig. 10. Many neighbouring grains show only marginally different orientations and

so for clarity we have colour coded the misorientation of the grain boundaries, rather than the orientation of the grains themselves. The corresponding histogram of correlated grain boundary misorientations is shown in Fig. 11. Unlike the low undercooling regime, the orientation histogram for which (not shown) displays a random (Mackenzie [28]) distribution of grain boundary orientations, the EBSD map now shows that there is a definite predominance of grain boundaries misorientations around 0 and 60°, even when the potentially unreliable determinations for misorientations < 1° are removed from the data set. The differences between the high and low undercooling samples is further reinforced by EBSD pole figure plots obtained for samples undercooled by 110 K and 192 K respectively (Fig. 12), which indicate a preferred texture at high undercooling which is not present at low undercooling.

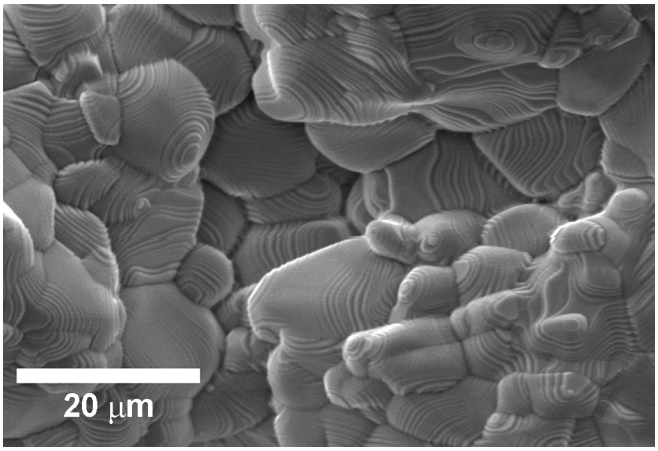

Figure 9 SEM micrograph of the inner surface of an open pore on the surface of a sample undercooled by 234 K prior to nucleation of solidification. Step like facets are clearly evident on many grains

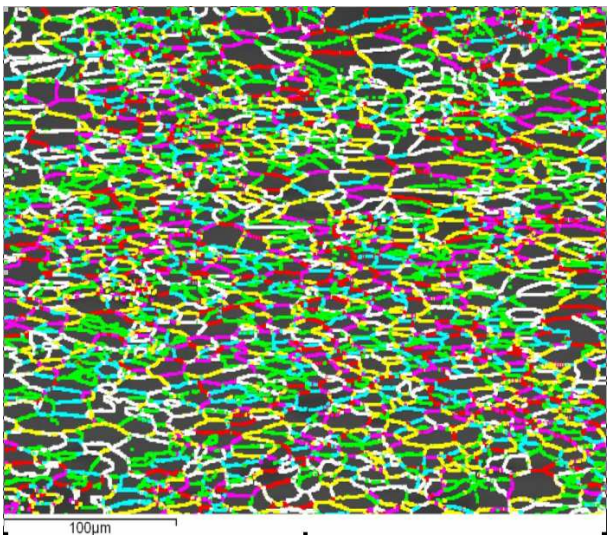

Figure 10 EBSD micrograph showing relative misorientation across grain boundaries within a sample undercooled by 192 K prior nucleation of solidification. Colour scale is 0 - 10° green,10° - 20° blue, 20° - 30° red, 30° - 40° magenta, 40° - 50° yellow, 50° - 60° white

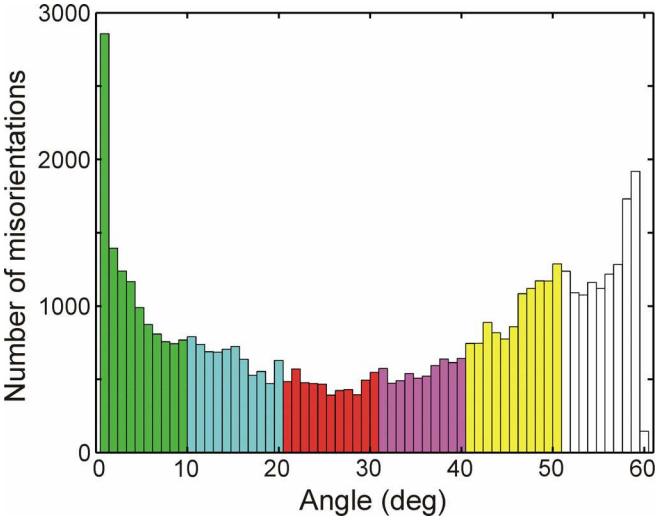

Figure. 11 Histogram of the correlated miscorientations across grain boundaries for the image shown in Fig. 10. Colour coding is the same as in the EBSD map

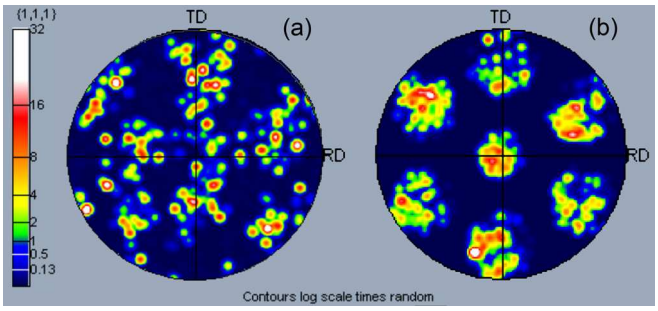

Figure 12 Pole figure plots in {111}direction, obtained from Ni_3Ge sample undercooled by (a) 110 K and (b) 192 K prior to nucleation of solidification. At high undercooling a much stronger texture across neighbouring grains is apparent than at low undercooling

Transmission electron microscopy has been used to look for APD's in these deeply undercooled samples however, no such evidence has been found. This is perhaps not surprising given the very low post-recalescence coolig rates that can be achieved during melt fluxing (typically of order 10 K s^{-1}) due to the high thermal mass of the flux, crucible, susceptor and heat shield relative to that of the sample. This would be consistent with *in situ* energy dispersive X-ray diffraction studies using synchrotron radiation on levitation undercooled Ni-Al which revealed that disordered superlattice structures can recrystallise to the ordered state on timescales of only a few seconds [29].

4. Discussion

βNi_3Ge is an ordered intermetallic compound displaying congruent melting in the composition range 22.5-25.0 at.% Ge. As such, it is a potentially simple system in which to study the transition from ordered to disordered growth with increasing departures from equilibrium. Growth velocity measurements made on a Ni-24at.% Ge

alloy over the undercooling range $57\ K \leq \Delta T \leq 362\ K$ appear to indicate that this material does indeed undergo a transition from slow, diffusion limited, growth to much more rapid, collision limited growth, with the critical undercooling for this transition being $\Delta T = 168\ K$. The growth velocity at this critical undercooling is $\approx 0.22\ m\ s^{-1}$, much lower than reported in other ordered intermetallics [8, 20, 21], but consistent with expected diffusive velocities in *fully ordered* superlattice structures [26]. The maximum growth velocity recorded in this material was $3.55\ m\ s^{-1}$.

Microstructural characterisation of the as-solidified, undercooled, samples also confirms that single phase βNi_3Ge is produced at all undercoolings. A change in solidification morphology is observed coincident with the break in the velocity-undercooling curve. Below the critical undercooling a coarse structure is observed, comprising a relatively small number of apparently randomly oriented grains. Such coarse grained polycrystalline structures are commonly found in undercooled samples in which solidification has been initiated with a trigger needle and are attributed to the contemporary initiation of a number of differently oriented dendrites at the contact point with the trigger [30]. As these would with propagate outwards from the contact area with similar velocities this is consistent with the results of the high speed imaging experiments performed on low undercooling samples, in which a single recalescence front is observed to move through the sample. Flow in the melt, evidence for which has previously been observed [31, 32] in materials processed via the flux encasement technique, may also contribute to the polycrystalline nature of the as-solidified material as a result of post-recalescence fragmentation of the dendritic skeleton.

Conversely, above the critical undercooling a much finer grain structure is observed. Similarly significant reductions in grain size above a critical undercooling have also been observed by Biswas et al. [21] in Fe- 18 at% Ge. In common with [21] we observe a high density of low angle grain boundaries which is consistent with a recovery process and we concur with their conclusion that the type of grain refinement observed in intermetallic systems such as Ni-Ge and Fe-Ge appears to be fundamentally different to the spontaneous grain refinement observed in solid solutions such as Ni-Cu [33] and Cu-O [34], which is generally considered to result from dendrite fragmentation [35, 36] or a growth instability mechanism [37, 38]. This view is supported by the texture observed across neighbouring grains. In spontaneous grain refinement observed in solid-solutions, any texture that was evident at lower undercooling [22, 34] is destroyed by the grain refinement process, resulting in a fine distribution of randomly oriented poles [34]. However, in Ni_3Ge the opposite is observed, with a random distribution of poles at low undercooling being replaced by strong texture in the highly undercooled, grain refined samples. Moreover, a large number of grain boundaries are observed around 60°, indicative of extensive twinning. No evidence of this was observed in Fe-Ge (compare Fig. 11 in this work with Fig. 6 in [21]), although such twinning has been observed in a number of other deeply undercooled metallic systems [39, 40]. In particular, in Ni-Ta alloys solidified at high undercooling under reduced gravity conditions during parabolic flight experiments [40], extensive twin boundaries were observed using EBSD analysis of the as-solidified samples. Their formation was attributed to dynamic recrystallisation due to shrinkage stress. This would be consistent with the observation that while the coarse grained structure obtained at low undercooling have undergone extensive cracking during post-solidification shrinkage, this is not observed in the grain refined samples

obtained at high undercooling. Instead many grains display a straight line step morphology which may be related to twin formation during recrystallisation, representing an alternative mechanism for accommodating post-solidification shrinkage stress [27].

We therefore believe that the most likely scenario is that for undercoolings below 168 K the melt solidified as the ordered $L1_2$ compound, while for undercoolings in excess of 168 K the melt initially solidified as a fully disordered compound and subsequently reordered as a consequence of recrystallisation due to shrinkage induced stress during slow post-recalescence cooling. The absence of APD's within grains would suggest that each grain contains only a single ordering, although the experimental evidence does not enable us to determine the relative timings of the grain refinement and ordering processes. However, we consider the most likely scenario is that the two processes are contemporaneous, with the crystallographic rearrangement required to reform the grain structure being accompanied by ordering.

5. Summary & Conclusions

The solidification of the congruently melting compound βNi_3Ge from its deeply undercooled parent melt has been studied using a melt fluxing technique. The main results from the study can be summarised as follows:

- Velocity-undercooling measurements have been made over the undercooling range $57\ K \leq \Delta T \leq 362\ K$. The maximum velocity recorded was $3.55\ m\ s^{-1}$
- The velocity-undercooling curve shows a clear signature for the transition from diffusion limited growth of the ordered compound at low undercooling to collision limited growth of the disordered compound at high undercooling. The transition undercooling was determined at $\Delta T \sim 168\ K$, wherein the growth velocity was $0.22\ m\ s^{-1}$, rather lower than other intermetallic systems where a similar transition is observed.
- Below the critical undercooling a relatively coarse structure comprising randomly oriented grains is observed. This structure appears to be subject to extensive cracking, probably due to post-solidification shrinkage.
- Above the critical undercooling a much finer grain structure is observed. Many of the grain boundaries display mis-orientations around 60º, which is suggestive of a twin relationship between grains, a relationship which is also evident in EBSD pole figures obtained from the deeply undercooled samples. The extensive cracking of the samples displayed in samples at low undercooling is no longer evident and is replaced by grains that display a straight line step morphology.
- We conjecture that below the critical undercooling of 168 K βNi_3Ge solidifies directly to the ordered compound. Above the critical undercooling growth is initially to the fully disordered compound. Slow post-recalescence cooling in the fluxing apparatus used to undercool the samples subsequently allows reordering of the structure and recrystallisation mediated by solidification shrinkage induced stress within the sample, resulting in a fine grained twinned structure.

6. References

1. Cahn RW, Siemers PA, Geiger JE, Bardham P (1987) The order-disorder transformation in Ni_3Al and Ni_3Al-Fe alloys: 1. Determination of the transition-temperatures and their relation to ductility. Acta Metall. 35:2737-2751.
2. Assadi H, Barth M, Greer AL, Herlach DM (1996) Microstructural development in undercooled and quenched Ni_3Al droplets. Mater. Sci. Forum 215-216:37-44.
3. Boettinger WJ, Aziz MJ (1989) Theory for the trapping of disorder and solute in intermetallic phases by rapid solidification. Acta Metall. 37:3379-3391.
4. Barth M, Wei B, Herlach DM (1995) Crystal-growth in undercooled melts of the intermetallic compounds FeSi and CoSi Phys. Rev. B 51:3422-3428.
5. Massalski TB (1983) Structure of Solid Solutions, Elsevier Sci. Publ., Amsterdam.
6. West JA, Aziz MJ (1992) Kinetic disordering of intermetallic compounds through 1^{st}-order and 2^{nd}-order transitions by rapid solidification, in A.R. Yavari (Ed.), Ordering & Disordering of Alloys, pp. 23-30, Elsevier Appl. Sci. Publ., Barking UK.
7. Assadi H, Greer AL (1997) Modelling of kinetics of solidification of intermetallic compounds. Mat. Sci. Eng. A 226:70-74.
8. Herlach DM (2001) Metastable materials solidified from undercooled melts. J. Phys. Condens. Mater. 13:7737-7751.
9. Inoue A, Tomioka H, Masumoto T (1983) Microstructure and mechanical-properties of rapidly quenched L12 alloys in Ni-Al-X systems. Metall. Trans. A 14:1367-1377.
10. Greer AL, Assadi H (1997) Rapid solidification of intermetallic compounds. Mater. Sci. Eng. A 226-228:133-141.
11. West JA, Manos JT, Aziz MJ (1991) Formation of metastable disordered Ni_3Al by pulsed laser-induced rapid solidification. Mater. Res. Soc. Symp. Proc. 213:859-864.
12. Vitta S, Greer AL, Somekh RE (1994) Rapid solidification of cobalt-titanium alloys induced by nanosecond laser-pulses. Mater. Sci. Eng. A 179:243-248.
13. Nash A, Nash P (1976) Binary Alloy Phase Diagrams. ASM, Ohio. US National Bureau of Standards Monograph Series 25, Vol 13 pp. 35.
14. Durand-Charre M (1998) The microstructure of superalloys. Gordon & Breach Science Publishers.
15. Brandt C, Inal OT (2002) Mechanical properties of Cr, Mn, Fe, Co, and Ni modified titanium trialuminides. J. Mater. Sci. 37:4399-4403.
16. Harada Y, Dunand DC (2000), Creep properties of Al_3Sc and Al_3(Sc, X) intermetallics. Acta Mater. 48:3477-3487.
17. Hill PJ, Adams N, Biggs T, Ellis P, Hohls J, Taylor SS, Wolff IM (2002) Platinum alloys based on Pt-Pt_3Al for ultra-high temperature use. Mater. Sci. Eng. 329:295-304.
18. Fang J, Schulson EM (1996) Microstructures of rapidly solidified powder and extruded rod of Ni_3Ge. Mater. Charact. 37:23-30.
19. Taub AI, Briant CL, Huang SC, Chang KM, Jackson MR (1986) Ductility in boron-doped, nickel-base L12 alloys processed by rapid solidification. Scripta Metall. 20:129-134.
20. Phanikumar G, Biswas K, Funke O, Holland-Moritz D, Herlach DM, Chattopadhyay K (2005) Solidification of undercooled peritectic Fe-Ge alloy. Acta Mater. 53:3591-3600.

21. Biswas K, Phanikumar G, Holland-Moritz D, Herlach DM, Chattopadhyay K (2007) Disorder trapping and grain refinement during solidification of undercooled Fe-18 at% Ge melts. Phil. Mag. 87:3817-3837.
22. Battersby SE, Cochrane RF, Mullis AM (1999) Growth velocity-undercooling relationships and microstructural evolution in undercooled Ge and dilute Ge-Fe alloys. J. Mater. Sci. 34:2049-2056.
23. Battersby SE, Cochrane RF, Mullis AM (1997) Highly undercooled germanium: Growth velocity measurements and microstructural analysis. Mater. Sci. Eng. A 226:443-447.
24. Dragnevski K, Cochrane RF, Mullis AM (2004) The mechanism for spontaneous grain refinement in undercooled pure Cu melts. Mater. Sci. Eng. A 375-377:479-484.
25. Dragnevski K, Cochrane RF, Mullis AM (2002) Experimental Evidence for Dendrite Tip Splitting in Deeply Undercooled, Ultra-High Purity Cu. Phys. Rev. Lett. 89:215502.
26. Reutzel S, Hartmann H, Galenko PK, Schneider S, Herlach DM (2007) Change of the kinetics of solidification and microstructure formation induced by convection in the Ni-Al system. Appl. Phys. Lett. 91:041913.
27. Herley PJ, Greer AL, Jones W (2001) Hillock formation on copper at room temperature by cleaning in ammonia vapour. Appl. Phys. Lett. 79:2725-2727.
28. Mackenzie JK (1964) The distribution of rotation axes in a random aggregate of cubic crystals, Acta Metall. 12:223.
29. Hartmann H, Holland-Moritz D, Galenko PK, Herlach DM (2009), Evidence of the transition from ordered to disordered growth during rapid solidification of an intermetallic phase. EPL 87:40007.
30. Volkmann T, Johannsen N, Herlach DM (2011) Dendritic growth velocities and growth morphologies in undercooled melts of pure Fe and Ni. Oral presentation at 3rd International Conference on Advances in Solidification Processes, 7-10 June 2011, Aachen, Germany.
31. Dragnevski K, Mullis AM, Walker DJ, Cochrane RF (2002) Mechanical deformation of dendrites by fluid flow during rapid solidification. Acta Mater. 50:3743-3755.
32. Mullis AM, Walker DJ, Battersby SE, Cochrane RF (2001) Deformation of dendrites by fluid flow during rapid solidification. Mater. Sci. Eng. A 304-306:245-249.
33. Willnecker R, Herlach DM, Feuerbacher B (1989) Evidence of nonequilibrium processes in rapid solidification of undercooled metals. Phys. Rev. Lett. 62:2707-2710.
34. Battersby SE, Cochrane RF, Mullis AM (2000) Microstructural evolution and growth velocity-undercooling relationships in the systems Cu, Cu-O and Cu- Sn at high undercooling. J. Mater. Sci. 35:1365-1373.
35. Schwarz M, Karma A, Eckler K, Herlach DM (1994) Physical-mechanism of grain-refinement in solidification of undercooled melts. Phys. Rev. Lett. 73:1380-1383.
36. Mullis AM (1997) Rapid solidification within the framework of a hyperbolic conduction model. Int. J. Heat Mass Transfer 40:4085-4094.
37. Mullis AM, Cochrane RF (1997) Grain refinement and the stability of dendrites growing into undercooled pure metals and alloys. J. Appl. Phys. 82:3783-3790.
38. Mullis AM, Cochrane RF (2001) A phase field model for spontaneous grain refinement in deeply undercooled metallic melts. Acta Mater. 49:2205-2214.

39. Dragnevski K, Cochrane RF, Mullis AM (2004) The solidification of undercooled melts via twinned dendritic growth, Metall. Mater. Trans. 35A:3211-3220.
40. Kolbe M, Lierfeld T, Wu Z, Eggeler G, Galenko P, Herlach DM (2011) Microstructure analysis of undercooled Ni-Ta alloys, Oral presentation at 3rd International Conference on Advances in Solidification Processes. 7-10 June 2011, Aachen, Germany.